# VLP-KAN: Low-Complexity and Interpretable RSS-Based VLP Using Kolmogorov-Arnold Networks

Fabian Seguel, Driton Salihu, Stefan Hägele and Eckehard Steinbach
Technical University of Munich, School of Computation, Information and Technology,
Department of Computer Engineering, Chair of Media Technology, Munich Institute of
Robotics and Machine Intelligence (MIRMI), 80333 München, Germany.

***Abstract*—Received signal strength (RSS)-based Visible Light Positioning (VLP) has gained attention due to its relatively easy infrastructure deployment and high localization accuracy. Different low-complexity geometrical and machine learning (ML)-based models have been proposed for localization because of their robustness against the uncertainty produced by tilted devices, non-Lambertian sources, and the low dimensionality of RSS-vector. Inspired by the Kolmogorov-Arnold representation theorem, Kolmogorov-Arnold Networks (KANs) have been proposed as a promising alternative to Multi-Layer Perceptrons (MLPs). This paper evaluates the use and performance of KANs in VLP systems for the first time. Results show that in the proposed scenario, KANs achieve below cm-level accuracy. Moreover, symbolic regression (SR) can be implemented straightforwardly to find a function that relates RSS with distance. It is shown in this paper that both KANs and SR-KAN models outperform MLP and Weighted K-nearest neighbors based approaches.**

***Index Terms*—Indoor Positioning, Visible light positioning, fingerprint, Deep Learning (DL)**

## I. Introduction

Due to the rapid proliferation of mobile devices and the associated location-based services, the issue of indoor localization has emerged as a critically important problem. Indoor Positioning Systems (IPS) operate within a complex environment. Moreover, the need for indoor localization systems emerged due to the absence of GPS coverage in such environments [1]. Various signals, including radio-frequency (RF), acoustics, and infrared, have been actively researched for indoor positioning applications. Among these, visible light positioning (VLP) has been identified as a promising technology that can cope with the requirements for localization in indoor environments. VLP uses modulated artificial light sources to provide wireless communications along positioning [2], [3]. These indoor positioning systems provide multiple advantages over other signals, such as no interference in RF-crowded areas, low energy consumption, increased security features, and the deployed lighting infrastructure, which can be reused as transmitters, leading to a low deployment cost. VLP algorithms rely on various signal parameters such as angle of arrival (AoA), time difference of arrival (TDoA), phase difference of arrival, or Received Signal Strength (RSS). Commonly, multiple light sources are used as transmitters. The receiving element of the VLP system could be a single photodiode (PD), a PD array, or a camera.

State-of-the-art VLP methods provide high precision. Nonetheless, depending on the application, these methods might have to increase their accuracy, robustness, and latency [4] as they are tested mostly in ideal scenarios. To improve the performance and robustness of RSS-based VLP systems, supervised machine learning (ML) methods are used. These methods do not require prior knowledge of the physical model or parameter estimation techniques to perform localization [5]. These ML techniques learn in a supervised manner the relation between RSS readings and the position directly from the data. Among the approaches used in the literature are multi-layer perceptrons (MLP) and polynomial fitting functions [6]–[8]. Most of the approaches found in the literature assume horizontal LED lights pointing directly downward. Nonetheless, such an assumption does not hold in some indoor scenarios where LED luminaries can be mounted in the ceiling arbitrarily tilted and rotated [4] as depicted in Fig. 1.

Recently, Kolmogorov-Arnold Networks (KANs) have been proposed as a promising alternative to MLPs [9]. While the universal approximation theorem inspires MLP, the KAN focuses on the Kolmogorov-Arnold representation theorem [10], [11]. Like MLPs, KANs have fully-connected structures. However, while MLPs place fixed activation functions on nodes (“neurons”), KANs place learnable activation functions on edges (“weights”). These networks have shown, in some cases, higher accuracy and interpretability than traditional MLPs when dealing with small-scale AI problems [9].

This paper presents the design and implementation of KANs specifically tailored to operate in RSS-based VLP. We evaluate the performance of the proposed methods in a simulated indoor environment comprised of 4 LED transmitters and a single photodetector (PD) receiver. The main contributions of this paper are as follows:

- We design and implement a KAN suitable for the problem of VLP. Different input and output scaling functions and KAN architectures are proposed.
- We use the potential of KANs to create a symbolic regression (SR)-based model that relates the received power with the distance and measure the SR-based model performance for indoor positioning.
- We compare the performance of the proposed method to state-of-the-art algorithms.


ISBN: 978-3-903176-71-3

The rest of the paper is organized as follows: Section 2 describes the principles of KAN. Section 3 details the scenario and the KANs optimization procedure. In Section 4, our results are presented and discussed. Finally, in Section 5, the main conclusions of the paper are presented.

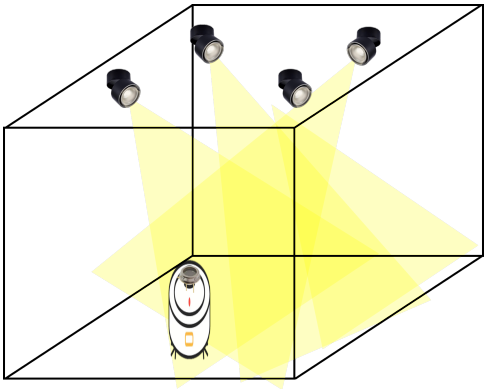

Fig. 1. Proposed scenario for the evaluation of the VLP-KAN.

## II. KANs

KANs Are based on the Kolmogorov-Arnold representation theorem [9]–[11]. This theorem states that if $f$ is a multivariate continuous function of $\mathbf{x}$ on a bounded domain, then it can be written as a finite composition of multiple continuous functions of a single variable and the binary operation of addition as:

$$f(\mathbf{x}) = f(x_1, x_2, \ldots, x_n) = \sum_{q=1}^{2n+1} \Phi_q \left( \sum_{p=1}^{n} \phi_{q,p}(x_p) \right), \quad (1)$$

where $f : [0,1] \longrightarrow \mathbb{R}$, $\phi_{q,p} : [0,1] \longrightarrow \mathbb{R}$, $\Phi_q : \mathbb{R} \longrightarrow \mathbb{R}$, $q = 1, 2, \ldots, n_{out}$ represents the $n_{out}$-dimensional output and $p = 1, 2, \ldots, n_{in}$ the $n_{in}$-dimensional input. One main drawback of this representation is that the 1D function in Eq. (1) can be non-smooth or fractal. Due to this, there might be functions that are non-learnable in practice. However, using deeper representations may bring the advantages of smoother activation functions and learn more complex representations. The expression in Eq. (1) is expressed in matrix form to implement and generalize this theorem to a network of any particular depth. In the particular case of RSS-based VLP, the supervised learning task consists in finding the composition of functions that relate the input RSS vector, **RSS**, to a particular distance $d$ between transmitter $j$ and receiver $i$, $d_{ji}$, i.e., $d_{ji} \approxeq f(\mathbf{RSS}) = \hat{d}_{ji}$.

To find this composition of functions, a neural network that explicitly parametrizes the functions $\phi_{q,p}$ and $\Phi_q$ of Eq. (1) needs to be defined. Many different parametrizable 1D functions can be used as basis functions. In particular, we use a B-spline curve with learnable coefficients of local B-spline basis functions. A B-spline is a piecewise polynomial spline expressed for a particular basis. Pieces meet with continuity as high as possible, given the degree of the basis. B-spline curve sections meet and connect in points called knots. The knot set can be expressed as $\mathcal{X} = \{x_0, x_1, \ldots, x_{K+1}\}$. The B-spline of order $m$ with knot sequence $\mathcal{X}$ is, by definition, a linear combination of basis B-splines functions of order $m$, $B_{k,m}(x), x \in [x_0, x_{K+1}]$, $k \in \mathbb{Z} = \{0, 1, \ldots, K+1\}$, which are associated with the knot sequence $\mathcal{X}$ denoted by:

$$S(x) = \sum_{k=0}^{K+m} a_k B_{k,m}, \quad (2)$$

where $a_k \in \mathbb{R}$ are the control points and $B_{k,m}$ are the normalized B-spline blending functions described by the order $m$ and the non decreasing real numbers $k$.

One key assumption for our approach is that the function relating the RSS readings to a particular distance between transmitter and receiver is learnable by a KAN of an arbitrary depth since the optical transmission model follows the laws of physics. These problems are often smooth and have sparse compositional structures, which facilitates the deployment of smooth Kolmogorov-Arnold representations [9].

The structure of a 3-layer KAN is shown in Fig. 2. The main breakthrough proposed by Liu et al. [9] is that they define a KAN layer with $n_{in}$ inputs and $n_{out}$ outputs as a matrix of 1D functions:

$$\mathbf{\Phi}_L = \begin{bmatrix} \phi_{1,1} & \cdots & \phi_{1,n_{in}} \\ \vdots & \ddots & \vdots \\ \phi_{n_{out},1} & \cdots & \phi_{n_{out},n_{in}} \end{bmatrix}, \quad (3)$$

where the functions $\phi_{q,p}(.)$ have trainable parameters.

The Eq. (1) is a composition of two KAN layers, the first one with $n_{in} = n$ and $n_{out} = 2n + 1$ and the second layer with $n_{in} = 2n + 1$ and $n_{out} = 1$. To generalise, a $L$-layers KAN for a given input vector $\mathbf{x} \in \mathbb{R}^{n_0}$ is given by:

$$f(\mathbf{x}) = (\mathbf{\Phi}_{L-1} \cdot \mathbf{\Phi}_{L-2} \cdot \ldots \cdot \mathbf{\Phi}_1 \cdot \mathbf{\Phi}_0) \cdot \mathbf{x} \quad (4)$$

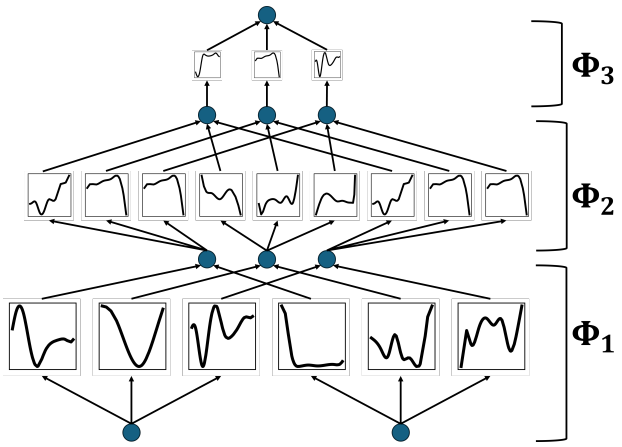


Fig. 2. 3-layer Kolmogorov-Arnold Network (KAN) architecture. The KAN shown has two inputs, one output, and one hidden layer.


ISBN: 978-3-903176-71-3

### A. SR-KAN

One of the main advantages of KANs is that they can be easily interpreted and transformed into mathematical formulas or expressions. SR can be used to discover the underlying mathematical relationship within the data. Traditional SR approaches search for the best mathematical expression within a large formula space. This process is computationally intensive and struggles with computational resource constraints [9]. The process of transforming a KAN to an SR model is as follows: each layer of the KAN is passed through a symbolification process. The activation functions of the KAN, which were found after training, are transformed into a symbolic form. For this, we consider a set of functions, $\mathcal{F} = \{\cos(x), \log(x), \ldots, \sqrt{(x)}\}$ . KAN layers cannot directly set the activation function to the exact symbolic formula since its inputs and outputs may have shifts and scaled versions of the function set. To overcome this problem, the symbolification process fits affine parameters $(a, b, c, d)$ to all the functions contained in $\mathcal{F}$, such that $y \approxeq cf(ax + b) + d, f \in \mathcal{F}$. The fitting is done by iterative grid search of a, b, and linear regression. Once the affine parameters are adjusted for each one of the functions in $\mathcal{F}$, the one with the highest coefficient of determination is selected.

## III. Proposed scenario and method

In this section, we introduce the considered scenario for testing the proposed method and provide details on the KAN architecture used for indoor visible light positioning. In Fig. 1, the proposed setup is shown. Here, 4 LEDs are used as transmitters, and a single PD receiver is considered at the mobile node side.

The VLC channel is modeled assuming line of sight (LOS) conditions. We assume that each LED transmitter $LED_j$ transmits an optical signal with a different frequency to the receiver $i$. The received power from transmitter $j$ at the photodetector (PD) $i$, $P_{ji}$, can be modeled as [12]:

$$P_{ji} = R_i P_j H_{ji}^{LOS} + R_i P_j H_{ji}^{n-LOS} + \eta, \tag{5}$$

where $P_j$, $R_i$, $H_{ji}^{LOS}$, $H^{n-LOS}$ and $\eta$ are the transmitted power, PD responsivity, optical LOS channel gain, non-LOS channel gain, and noise, respectively. As depicted in Fig. 3 (a), the optical channel gain $H_{ij}^{LOS}$ can be modelled as:

$$H_{ji}^{LOS} = \begin{cases} \frac{C_{ji}}{d_{ji}^2} \cos^{m_j}(\varphi_{ji}) \cos(\psi_{ji}) & 0 \le \psi_{ji} \le \Psi_i \\ 0 & \text{elsewhere} \end{cases}, \tag{6}$$

where $d_{ji}^2$ is the distance between transmitter and receiver, $m_j$ is the Lambertian order of the transmitter, $\psi_{ji}$ is the transmission angle with respect to the normal $\hat{\mathbf{N}}_j$, $\varphi_{ji}$ is the incident angle at the receiver with respect to the normal $\hat{\mathbf{N}}_i$ and $\Psi_i$ is the PD field of view (FOV). Finally, the constant $C_{ji} =$ can be modelled as:

$$C_{ji} = \frac{(m_j + 1)A}{2\pi} G(\psi_{ji}) T_s(\psi_{ji}), \tag{7}$$

where $A$ corresponds to the area of the PD and $G(\psi_{ij})T_s(\psi_{ij})$ represents the combined optical filter gain and the optical concentrator gain.

In a real setup, the transmitter and receivers might be tilted. Due to this, the incident and transmitted angles in Eq. (6) can be determined using the following expressions:

$$d_{ji} = ||\mathbf{r}_j - \mathbf{r}_i||, \tag{8}$$

$$cos(\varphi_{ji}) = \hat{\mathbf{N}}_j \cdot \left( \frac{\mathbf{r}_j - \mathbf{r}_i}{d_{ji}} \right), \tag{9}$$

$$cos(\psi_{ji}) = \hat{\mathbf{N}}_i \cdot \left( \frac{\mathbf{r}_i - \mathbf{r}_j}{d_{ji}} \right). \tag{10}$$

The PD and LED normal vectors can be calculated in spherical coordinates, assuming $\beta$ is the tilt angle and $\alpha$ is the rotation angle, as depicted in Fig. 3.

$$\hat{\mathbf{N}}_i = \frac{[\sin(\beta_i)\cos(\alpha_i), \sin(\beta_i)\sin(\alpha_i), \cos(\beta_i)]}{\|[\sin(\beta_i)\cos(\alpha_i), \sin(\beta_i)\sin(\alpha_i), \cos(\beta_i)]\|_2}, \tag{11}$$

As the transmitter is assumed to be always pointing downwards, the tilting angle of the transmitter $j$ is restricted in the range of $\pi/2 \le \beta_j^{total} \le 3\pi/2$. Using this assumption, we define the tilting angle of the transmitter with respect to the normal vector $\hat{\mathbf{N}}_g$ as $\beta_j^{total} = \pi + \beta_j$, where $-\pi/2 \le \beta_j \le \pi/2$. Using the trigonometric identity of the sum of two angles, it can be demonstrated that $\cos(\beta_j^{total}) = \cos(\pi + \beta_j) = -\cos(\beta_j)$. Using this, we define the normal vector to the transmitter plane using the tilting angle $\beta_j$ instead of $\beta_j^{total}$ as follows:

$$\hat{\mathbf{N}}_j = \frac{[\sin(\beta_j)\cos(\alpha_j), \sin(\beta_j)\sin(\alpha_j), -\cos(\beta_j)]}{\|[\sin(\beta_j)\cos(\alpha_j), \sin(\beta_j)\sin(\alpha_j), \cos(\beta_j)]\|_2}. \tag{12}$$

We assume the PD is horizontal to the floor plane, i.e., $\beta_i = 0$. This assumption holds in various practical applications [13]. furthermore, using this assumption, the incidence angle to the PD, $\psi_{ji}$, is rotation-invariant. This article assumes that the LED transmitters are arbitrarily tilted and rotated, as might happen in some ceiling-mounted lighting architectures [4].

Similarly, the non-LOS channel gain shown can be mathematically expressed as [14]:

$$H_{ij}^{n-LOS} = \begin{cases} \sum_{w=1}^{W} H_{jw} H_{wi} & 0 \le \psi_{wi} \le \Psi_i \\ 0 & \text{elsewhere} \end{cases}, \tag{13}$$

where $H_{jw}$ is the channel gain from LED to the wall, $H_{wi}$ is the channel gain from wall to PD, and $W$ is the total number of reflective elements considered in the algorithm. In particular, the channel gain from the LED to the reflective element and from the reflective element to the PD is obtained as follows:

$$H_{jw} = \frac{\Delta A_w \rho_w}{d_{jw}^2} cos^{m_l}(\phi_{jw}) \cos(\psi_{jw}), \tag{14}$$

$$H_{wi} = C_{wi} \cos(\phi_{wi}) \cos(\psi_{wi}), \tag{15}$$

where $\Delta A_w$ is the area of the considered reflecting element, $\rho_w$ is the reflecting coefficient of the surface area $\Delta A_w$, $d_{jw}$


ISBN: 978-3-903176-71-3

is the distance between the source and the reflective element as shown in Fig. 3 (b). The angle $\psi_{jw}$ is the transmission angle with respect to the normal $\hat{\mathbf{N}}_j$ of the reflecting element, $\varphi_{jw}$ is the incident angle at the reflecting surface with respect to the normal $\hat{\mathbf{N}}_w$, $\psi_{wi}$ is the reflected angle with respect to the normal $\hat{\mathbf{N}}_w$, and $\varphi_{wi}$ is the incident angle at the PD with respect to the normal $\hat{\mathbf{N}}_i$ of the ray coming from the reflected element.

Since $||H^{(k)}_{non-LOS}|| \to 0$ when $k \to \infty$, the channel impulse response can be modeled using only the first reflection. The first reflection is the most important component since it limits the data rate in LOS transmissions. The VLC system parameters used for simulation are shown in Table I.

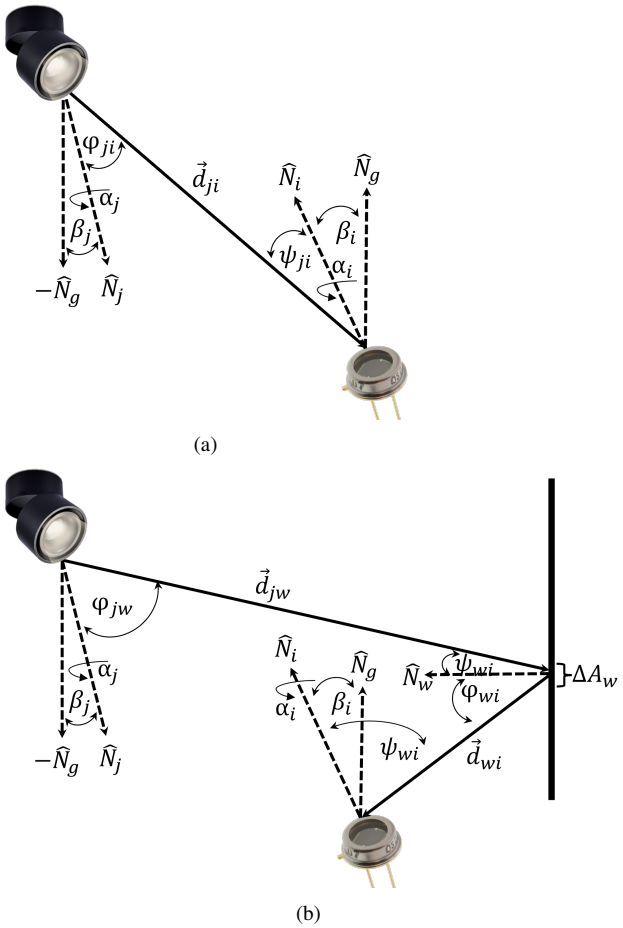


Fig. 3. Tilted photodiode and LED source for (a) LOS link and (b) non-LOS link.

To evaluate the performance of the KANs, first, a few parameters must be found to optimize its performance. B-spline coefficients are found in the training stage using the backpropagation algorithm. Nonetheless, three other parameters have to be tuned beforehand. The first one is called the grid size or number of knots. The second parameter is the number of hidden layers and the number of functions of each layer. Finally, the degree of the spline base function $d$ needs to be selected.

We perform a grid search with the parameters in Table II.

TABLE I
VLC SYSTEM PARAMETERS

| Parameter | Value | Parameter | Value |
|---|---|---|---|
| LED half power | $60°$ | Source power | $10\,(W)$ |
| Area of PD | $10^{-4}\,(m^2)$ | $T_s(\psi_{ij})$ | 1 |
| FOV receiver | $90°$ | Room | $3 \times 3\,(m)$ |
| LED height | $3\,(m)$ | $G(\psi_{ij})$ | 1 |
| Number of LEDs | 4 | PD height | $1.5\,(m)$ |
| Grid train | $0.5\,(m)$ | Grid test | $0.11\,(m)$ |
| System BW | $10\,(MHz)$ | Noise PSD | $10^{-21}\,(W/Hz)$ |
| $\Delta A_w$ | $0.0625\ (m^2)$ | $\rho_w$ | 0.8 |

TABLE II
GRID SEARCH PARAMETERS FOR KAN ARCHITECTURE.

| knots | L | $n_{out}$ | $d$ |
|---|---|---|---|
| [3,10,20,50] | [1,2,3,4] | [1,2,3] | [3] |

The selected fitness function to optimize B-spline coefficients is the mean squared error (MSE).

It has to be noticed that the input and output of the KAN are both bounded by:

$$0 \preceq \mathbf{RSS} \preceq \mathbf{RSS}_{max}, \tag{16}$$

$$\mathbf{r}_{min} \preceq \mathbf{r}_i \preceq \mathbf{r}_{max}, \tag{17}$$

where $\mathbf{r}_{min} = [\min(r_x), \min(r_y)]$, and $\mathbf{r}_{max} = [\max(r_x), \max(r_y)]$ are the minimum and maximum coordinates of the room. The input and output size is determined by the number of lights inside the room. The input of our $KAN$ is: $\mathbf{RSS} \in \mathbb{R}^4$ and the output: $KAN(\mathbf{RSS}) = \hat{d}_{ji} \approxeq d_{ji} \in \mathbb{R}$ is the distance between transmitter and receiver. Once the distance is computed, the mobile node position can be obtained using the least squares method as follows:

$$\begin{aligned} \underset{\hat{\mathbf{r}}_i}{\text{minimize}} \quad & \sum_{j=1}^{J} \left( ||\mathbf{r}_j - \hat{\mathbf{r}}_i|| - \hat{d}_{ji} \right)^2 \\ \text{subject to} \quad & \hat{\mathbf{r}}_i \succeq \mathbf{r}_{min}, \\ & \hat{\mathbf{r}}_i \preceq \mathbf{r}_{max}. \end{aligned} \tag{18}$$

From Eq. 18, it can be seen that this requires knowledge of the position of the LED transmitters $\mathbf{r}_j$ while tilting and rotation angles of the transmitter are unknown and directly learned by the KAN in a supervised manner.

## IV. RESULTS AND DISCUSSION

In this section, we show the performance of the proposed KAN in the RSS-based VLP problem. As shown in Fig. 4, there is a direct relationship between the RSS and the distance between LED 1 and the PD when no tilted LEDs are considered. An exponential function is often fitted to relate the RSS and the distance before performing circular trilateration. In this scenario, the distance based on RSS can be found by employing the following expression:

$$\hat{d}_{ji} = \left( \frac{(m+1)AP_j h_i^{m+1}}{2\pi P_{ji}} \right)^{\frac{1}{m+3}} = \left( \frac{a}{P_{ji}} \right)^b, \tag{19}$$


ISBN: 978-3-903176-71-3

where $a = \left(\frac{(m+1)AP_j h_i^{m+1}}{2\pi}\right)$ and $b = \frac{1}{m+3}$. The above expression can be converted using the logarithmic function as follows:

$$\log\left(\hat{d}_{ji}\right) = b\log(a) - b\log(P_{ji}) = c - b\log(P_{ji}). \quad (20)$$

Based on this derivation, we can conclude that using the logarithmic function, the expression that relates the distance and the RSS can be written into a linear function instead of the original expression. We will measure the effect of such transformation on the training and test data when using a simple one-layer KAN.

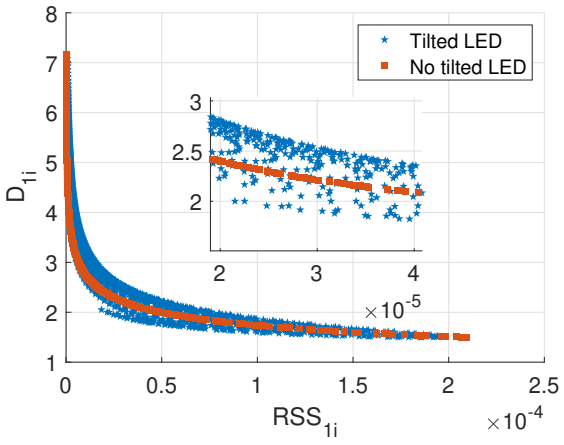


Fig. 4. Distance vs RSS relationship for tilted LED and horizontal LED.

In Fig. 4, it can also be seen that the above-described relationship does not hold when the LEDs installed in the ceiling are tilted as the function becomes not injective and more complex. To solve this problem, the RSS from different LEDs relate a particular **RSS** vector to a distance. Up to date, there is no analytical solution for this function. Due to this, traditional ML models have been used to estimate this distance by relying on the universal approximation theorem of neural networks.

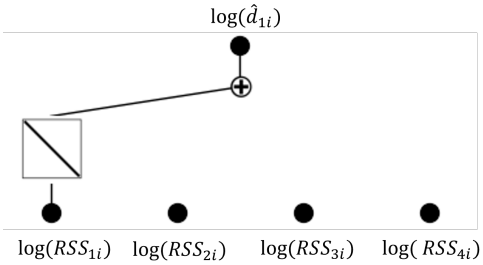


Fig. 5. Trained 1 Layer KAN [4,1] for estimation of $d_{1i}$ using T10.

### A. Impact of signal pre-processing

As mentioned before, the functions that relate the RSS to the distance between transmitter and receiver can be expressed in more than one manner based on the transformation applied to the Eq. (19). In this section, we will measure the impact of signal pre-processing on the performance of a simple KAN model. We consider only the simplest VLP case, i.e., no tilted transmitters or receivers. In Table III, the error on the test dataset after applying scaling, $\mathcal{S}()$, and $log()$ functions is displayed. The scaling function used here is the min-max normalization, which re-scales the features in the $[-1, 1]$ range.

TABLE III
PERFORMANCE OF ONE LAYER KAN TO DIFFERENT INPUT AND OUTPUT PRE-PROCESSING.

| Transform | Input | Output | MSE KAN [4,1] |
|---|---|---|---|
| T1 | **RSS** | $d_{ji}$ | $1.62 \times 10^{-1}$ |
| T2 | **RSS** | $\log(d_{ji}))$ | $3.78 \times 10^{-2}$ |
| T3 | **RSS** | $\mathcal{S}(d_{ji})$ | $4.27 \times 10^{-2}$ |
| T4 | **RSS** | $\mathcal{S}(\log(d_{ji}))$ | $6.70 \times 10^{-2}$ |
| T5 | $\mathcal{S}$(**RSS**) | $d_{ji}$ | $1.77 \times 10^{-2}$ |
| T6 | $\mathcal{S}$(**RSS**) | $\log(d_{ji})$ | $8.98 \times 10^{-2}$ |
| T7 | $\mathcal{S}$(**RSS**) | $\mathcal{S}(d_{ji})$ | $3.92 \times 10^{-2}$ |
| T8 | $\mathcal{S}$(**RSS**) | $\mathcal{S}(\log(d_{ji}))$ | $6.29 \times 10^{-2}$ |
| T9 | log(**RSS**) | $d_{ji}$ | $2.34 \times 10^{-5}$ |
| T10 | log(**RSS**) | $\log(d_{ji})$ | $\mathbf{3.7 \times 10^{-7}}$ |
| T11 | log(**RSS**) | $\mathcal{S}(d_{ji})$ | $1.12 \times 10^{-2}$ |
| T12 | log(**RSS**) | $\mathcal{S}(\log(d_{ji}))$ | $7.32 \times 10^{-3}$ |
| T13 | $\mathcal{S}$(log(**RSS**)) | $d_{ji}$ | $2.77 \times 10^{-2}$ |
| T14 | $\mathcal{S}$(log(**RSS**)) | $\log(d_{ji})$ | $5.5 \times 10^{-3}$ |
| T15 | $\mathcal{S}$(log(**RSS**)) | $\mathcal{S}(d_{ji})$ | $1.76 \times 10^{-3}$ |
| T16 | $\mathcal{S}$(log(**RSS**)) | $\mathcal{S}(\log(d_{ji}))$ | $\mathbf{9.57 \times 10^{-7}}$ |

As it can be seen in Table III, the proposed KAN model achieves the best performance when the logarithmic transform is applied to the RSS and distance (T10). As was shown in Eq. (20), the log transforms the original exponential relationship between RSS and distance into a linear equation. Due to this, the performance of the KAN is increased by simplifying the function to be found using simple pre-processing. This finding will be crucial in the remainder of the paper as these transforms will be applied to the input and output signals to find a function that describes the distances based on RSS readings when tilted LEDs are considered.

It can also be seen in Fig. 5 that the network is capable of pruning unnecessary inputs, and only one RSS value is required to estimate the distance between the first transmitter and the receiver. Here, the distance estimation to LED 1 is performed using only the RSS information coming from itself. By applying SR in this KAN, we obtain that the proposed model follows the equation $\log(d_{1i}) = -0.2\log(RSS_{1i}) - 1.29$. This expression has the same structure as Eq. (20). Here, for the first time, we show the capabilities of KANs and SR in finding an approximate polynomial expression for the problem of VLP.

### B. Performance with tilted LEDs

In this section, we show the performance of different KAN architectures to find the relationship between **RSS** and the distance between transmitter and receiver when tilted transmitters are considered. It can be noticed from Fig. 6 that the power distribution does not follow a circular coverage when tilted LEDs are considered. Due to this, the geometrical functions


ISBN: 978-3-903176-71-3

$$\log\left(\hat{d}_{11}\right) = -3.8549\sqrt{(0.0635x_1 - 0.00035x_3 + 0.0317(0.1222x_4+1)^2 + 1 + 0.0004e^{-0.3080x_2)}} + 0.3557sin(-0.0186x_2 + 0.0043x_4 + 0.49340(0.0933x_3+1)^2 + 0.2153sin(0.4159x_1 + 4.3999) + 2.1535) + 3.0172 \quad (21)$$

$$\log\left(\hat{d}_{21}\right) = -0.0689(-0.0040x_1 - 0.0269x_3 + 0.0071x_4 - sin(0.2127x_2 + 8.3839) - 0.9518)^2 + 1.4529sin(-0.0788x_2 + 0.0014x_3 + 1.2986(-0.0919x_1 - 1)^2 + 0.0225sin(0.4041x_4 + 9.6586) - 0.6192) - 0.1059 + 1.2539sin(0.0533x_2 + 7.3448e^{0.4479x_1} - 0.0391sin(0.6038x_3 + 8.4287) + 0.0196sin(0.5835x_4 - 0.9840) - 3.1224) \quad (22)$$

$$\log\left(\hat{d}_{31}\right) = -0.2094x_3 + 0.0220(0.2082x_2+1)^2 - 0.0585sin(0.3797x_1 + 8.2005) + 0.0550sin(0.3799x_4 - 7.5999) - 0.0199sin(1.5658(0.1162x_3+1)^2 + 7.5439sin(0.1804x_1 - 2.9925) - 0.4941sin(0.4125x_2 - 1.4039) + 1.6610sin(0.3799x_4 + 5.0) - 8.4558) - 1.4747 \quad (23)$$

$$\log\left(\hat{d}_{41}\right) = -0.0032x_1 - 0.0043x_2 + 0.0117x_3 - 0.1922x_4 - 0.6500(-0.1038x_2 - 1)^2 + 0.0830sin(0.2123x_4 + 4.7760) - 1.0989 + 0.0003e^{-0.4719x_1} \quad (24)$$

that relate the distance and the RSS cannot be obtained from Equations (19) and (20).

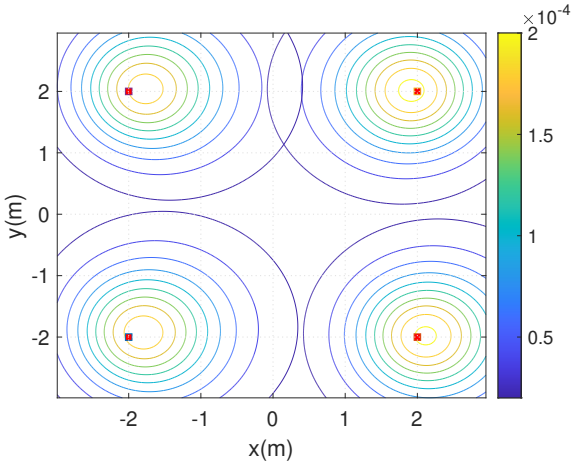


Fig. 6. Power distribution in the proposed scenario with tilted LEDs considering only LOS.

To discover the set of small functions that relate the **RSS** with a particular distance, we train different KANs with the parameters depicted in Table II. Table IV shows the LED's tilt and rotation angles considered in this scenario.

TABLE IV
TILT AND ROTATION ANGLES FOR EACH LED.

| **Rotation** | **Angle** | **Tilted** | **Angle** |
|---|---|---|---|
| $\alpha_1$ | 20° | $\beta_1$ | 20° |
| $\alpha_2$ | 10° | $\beta_2$ | 11° |
| $\alpha_3$ | 170° | $\beta_3$ | 8° |
| $\alpha_4$ | 10° | $\beta_4$ | 22° |

In Table V, the results of the best architecture for different numbers of KAN layers are shown.

The architecture without hidden layers is not a good fit for solving this problem. Due to this, more functions are required

TABLE V
PERFORMANCE OF DIFFERENT ARCHITECTURES FOR DISTANCE ESTIMATION WITH TILTED LEDS.

| $d_{ji}$ | **Layers** | **Architecture** | **MSE** ($\times 10^{-3}$) |
|---|---|---|---|
| $d_{1i}$ | 0 | [4,1] | 1.9 |
| $d_{1i}$ | **1** | **[4,2,1]** | **0.048** |
| $d_{1i}$ | 2 | [4,2,2,1] | 0.047 |
| $d_{2i}$ | 0 | [4,1] | 1.6 |
| $d_{2i}$ | **1** | **[4,3,1]** | **0.033** |
| $d_{2i}$ | 2 | [4,2,3,1] | 0.026 |
| $d_{3i}$ | 0 | [4,1] | 4.5 |
| $d_{3i}$ | **1** | **[4,2,1]** | **0.036** |
| $d_{3i}$ | 2 | [4,2,1,1] | 0.037 |
| $d_{4i}$ | 0 | [4,1] | 1 |
| $d_{4i}$ | **1** | **[4,2,1]** | **0.043** |
| $d_{4i}$ | 2 | [4,2,1,1] | 0.049 |

to minimize the distance estimation error. The MSE obtained by the 1 and 2 hidden layers architectures is lower than $5 \times 10^{-5}$.

This means that a combination of small functions is capable of estimating $\log(d_{ji})$ based on the vector $\log(\mathbf{RSS})$ with a single PD as receiver. It has to be noticed that the error obtained using the input and output data T1 in Table III is higher than $1 \times 10^{-2}$. This shows that the logarithmic transformation is an efficient step for improving the performance of the proposed method.

In Fig. 8, we show different trained KANs for the problem of estimating the distance to the LED 1 based on the RSS vector.

For simplicity, we select the simplest KAN that achieves an error lower than $1 \times 10^{-4}$. The above KAN architectures can be transformed into an approximated composition of polynomial functions using SR. This makes the implementation of the positioning method suitable for edge nodes where the computational power is restricted. Equations (21), (22), (23), and (24) show the SR functions obtained from the KAN that relate each RSSI to the distance. As can be seen, these functions can be implemented in any device without needing


ISBN: 978-3-903176-71-3

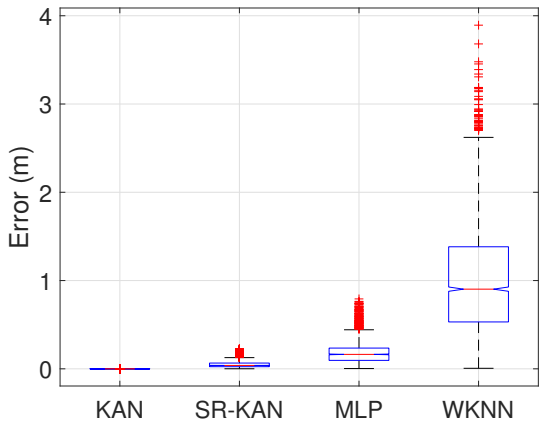


Fig. 7. Positioning error of the proposed method (KAN) compared to KAN-based SR expression, MLP [4], and WKNN [7].

high computational power or a high number of parameters.

### C. Performance on Positioning

Here, we measure the impact of the distance estimation error in the indoor positioning task. We compare the results obtained using a simple MLP and WKNN with the 3-layer KAN and the approximated composition of functions obtained by symbolic regression (SR-KAN). The MLP follows the same architecture proposed in [4], namely, two hidden layers of 6 and 3 nodes, respectively, while the WKNN method is the one proposed in [7]. In Fig. 7, we show that KAN can perform sub-centimeter positioning in the considered scenario. Furthermore, the approximated mathematical expression derived from it, SR-KAN, performs better than MLP and WKNN. This solution is also feasible for cm-level accuracy indoor positioning systems in edge devices that do not support deep-learning packages and functionalities.

As with other fingerprint-based positioning methods, the proposed KAN and SR-KAN suffer detrimental effects from changes in the scenario. These changes account for different tilted or rotation angles or LED power and position changes. Due to this, the model needs to be re-trained when these changes occur.

The proposed method uses one KAN for each LED light in the environment. Due to this, the number of KANs to be trained and SR-KAN models to be stored increases linearly with the number of LED transmitters within the environment.

## V. Conclusions and Future Work

In this paper, we proposed for the first time the usage of KANs for VLP. We consider the scenario where transmitters are tilted and rotated, and receivers are parallel to the floor plane. Through simulation, we show that the proposed method outperforms traditional MLP and WKNN in the task of indoor positioning when tilted transmitters and a single horizontal transmitter are considered. In future work, we will measure the performance of KANs in the task of device orientation determination when tilted transmitters and receivers are considered. Furthermore, multiple PD architectures will be proposed for device orientation and position determination. A measurement campaign using commercial off-the-shelf visible light communications devices will be conducted to measure the performance of the method in real-world scenarios.

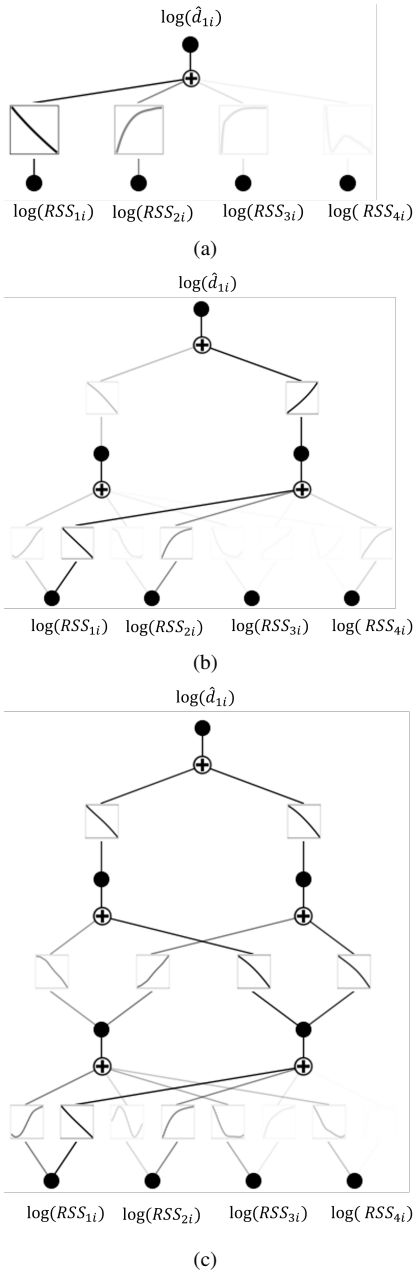


Fig. 8. Best trained KANs for the estimation of $d_{1i}$ with different sizes of hidden layers considering tilted LEDs (a) KAN=[4,1], (b) KAN=[4,2,1], and (c) KAN=[4,2,1,1].

## Acknowledgment

The authors acknowledge the financial support by the Federal Ministry of Education and Research of Germany in the programme of "Souverän. Digital. Vernetzt.". Joint project 6G-life, project identification number: 16KISK002.


ISBN: 978-3-903176-71-3

## REFERENCES


[1] F. Zafari, A. Gkelias, and K. K. Leung, "A survey of indoor localization systems and technologies," *IEEE Communications Surveys and Tutorials*, vol. 21, pp. 2568–2599, 2019.

[2] M. Afzalan and F. Jazizadeh, "Indoor positioning based on visible light communication: A performance-based survey of real-world prototypes," *ACM Computing Surveys*, vol. 52, 5 2019.

[3] J. Luo, L. Fan, and H. Li, "Indoor positioning systems based on visible light communication: State of the art," *IEEE Communications Surveys and Tutorials*, vol. 19, pp. 2871–2893, 10 2017.

[4] N. Knudde, W. Raes, J. D. Bruycker, T. Dhaene, and N. Stevens, "Data-efficient gaussian process regression for accurate visible light positioning," *IEEE Communications Letters*, vol. 24, pp. 1705–1709, 8 2020.

[5] H. Q. Tran and C. Ha, "Machine learning in indoor visible light positioning systems: A review," *Neurocomputing*, vol. 491, pp. 117–131, 6 2022.

[6] C. Carreño, F. Seguel, P. Charpentier, and N. Krommenacker, "Polynomial fitting functions for visible light positioning based on rss with tilted receiver," in *IPIN 2021 WiP Proceedings*, 2021.

[7] A. H. A. Bakar, T. Glass, H. Y. Tee, F. Alam, and M. Legg, "Accurate visible light positioning using multiple-photodiode receiver and machine learning," *IEEE Transactions on Instrumentation and Measurement*, vol. 70, 2021.

[8] V. P. Rekkas, S. Sotiroudis, D. Plets, W. Joseph, and S. K. Goudos, "Visible light positioning: A machine learning approach," *7th South-East Europe Design Automation, Computer Engineering, Computer Networks and Social Media Conference, SEEDA-CECNSM 2022*, 2022.

[9] Z. Liu, Y. Wang, S. Vaidya, F. Ruehle, J. Halverson, M. S. Soljači´c, T. Y. Hou, and M. Tegmark, "Kan: Kolmogorov-arnold networks," 4 2024.

[10] A. K. D. A. Nauk and undefined 1957, "On the representation of continuous functions of many variables by superposition of continuous functions of one variable and addition," *mathnet.ruAN KolmogorovDoklady Akademii Nauk, 1957•mathnet.ru*.

[11] J. Braun and M. Griebel, "On a constructive proof of kolmogorov's superposition theorem," *Constructive Approximation*, vol. 30, pp. 653–675, 11 2009.

[12] T. Komine and M. Nakagawa, "Fundamental analysis for visible-light communication system using led lights," *IEEE Transactions on Consumer Electronics*, vol. 50, pp. 100–107, 2 2004.

[13] F. Chen, N. Huang, N. Huang, C. Gong, and C. Gong, "Rss-based visible light positioning with unknown receiver tilting angle: robust design and experimental demonstration," *Optics Express, Vol. 30, Issue 22, pp. 39775-39793*, vol. 30, pp. 39775–39793, 10 2022.

[14] C. R. Lomba, R. T. Valadas, and A. M. de Oliveira Duarte, "Effcient simulation of the impulse response of the indoor wireless optical channel," *INTERNATIONAL JOURNAL OF COMMUNICATION SYSTEMS Int. J. Commun. Syst*, vol. 13, pp. 537–549, 2000.



ISBN: 978-3-903176-71-3